Insight into the f-Derived Fermi Surface of the Heavy-Fermion Compound $YbRh_2Si_2$

S. Danzenbächer,[1] D. V. Vyalikh,[1,*] K. Kummer,[1,2] C. Krellner,[3] M. Holder,[1] M. Höppner,[1] Yu. Kucherenko,[1,4] C. Geibel,[3] M. Shi,[5] L. Patthey,[5] S. L. Molodtsov,[6] and C. Laubschat[1]

[1]*Institut für Festkörperphysik, Technische Universität Dresden, D-01062 Dresden, Germany*
[2]*European Synchrotron Radiation Facility, BP 220, F-38043 Grenoble Cedex, France*
[3]*Max-Planck-Institut für Chemische Physik fester Stoffe, Nöthnitzer Strasse 40, D-01187 Dresden, Germany*
[4]*Institute for Metal Physics, National Academy of Sciences of Ukraine, UA-03142 Kiev, Ukraine*
[5]*Swiss Light Source, Paul Scherrer Institute, CH-5232 Villigen-PSI, Switzerland*
[6]*European XFEL GmbH, Albert-Einstein-Ring 19, D-22671 Hamburg, Germany*

(Received 9 June 2011; published 22 December 2011)

Angle-resolved photoelectron spectroscopy (ARPES) was used to study the Fermi surface of the heavy-fermion system $YbRh_2Si_2$ at a temperature of about 10 K, i.e., a factor of 2 below the Kondo energy scale. We observed sharp structures with a well-defined topology, which were analyzed by comparing with results of band-structure calculations based on the local-density approximation (LDA). The observed bulk Fermi surface presents strong similarities with that expected for a trivalent Yb state, but is slightly larger, has a strong Yb-4f character, and deviates from the LDA results by a larger region without states around the $\bar{\Gamma}$ point. These properties are qualitatively explained in the framework of a simple f-d hybridization model. Our analysis highlights the importance of taking into account surface states and doing an appropriate projection along $\boldsymbol{k}_z$ when comparing ARPES data with results from theoretical calculations.

DOI: 10.1103/PhysRevLett.107.267601 PACS numbers: 79.60.−i, 71.27.+a, 74.25.Jb

The Fermi surface (FS) is one of the most characteristic properties of a metal, separating occupied and unoccupied states at zero temperature and influencing thereby transport, electronic and magnetic properties of the solid. If electron correlation is negligible and electrons behave almost as independent particles like in simple metals [1], the Fermi surface may be described with the local-density approximation (LDA) and evaluated experimentally by angle-resolved photoelectron spectroscopy (ARPES) [2]. With increasing localization of the electron states, however, removal of electrons is related to large on-site Coulomb energies, which affect the photoemission process [3]. Furthermore the localization goes along with increasing correlation effects, which strongly influence the electronic states at the Fermi level (E_F) and may induce a large change in the FS, but which are not taken into account in the LDA. As a result, studying the Fermi surface of strongly correlated electron systems is a challenge both for experiments and for theory.

Prominent representatives of such systems are rare-earth intermetallics, in particular, Yb- and Ce-based systems, where the partly occupied 4f shell lies deep inside the ionic core and maintains most of its atomic properties in the solid. The lacking overlap between neighboring 4f orbitals leads in LDA to the formation of narrow bands around the E_F, which are formed by linear combination of states with atomic $4f^{n-l}(5d6s)^{2+l}$ configurations. Since changes of the 4f occupancy are usually related to large on-site Coulomb repulsion energies of the order of several eV, low-energy excitations are restricted to processes that leave the 4f occupation unaffected, i.e., intraatomic $f \rightarrow f$ and $(5d6s) \rightarrow (5d6s)$ transitions describing local magnetic excitations in an otherwise ordinary metal. In case of mixed-valent or Kondo systems, however, adjacent 4f configurations get energy degenerate and low-energy electron transitions between states of different 4f occupation become possible, influencing heavily the magnetic and transport properties. Periodic arrangements of Kondo impurities in a lattice cause heavy-fermion (HF) behavior characterized by effective masses of the charge carriers that are by a factor hundred or even thousand larger than that of a free electron [4]. An isolated Kondo impurity can be successfully handled within the single-impurity Anderson model [5], for the description of a Kondo lattice, the periodic Anderson model [6] should be applied. For this model, however, a satisfactorily solution is still missing due to problems of the correct handling of the large Coulomb repulsion energies. Hence, how the Fermi surface of a heavy-fermion system should be assessed and how it will be modified upon crossing the quantum critical point (QCP) separating the stable trivalent magnetic ground state from the paramagnetic Kondo screened ground state has remained rather unclear.

At zero temperature one expects, based on the Luttinger theorem, that the Fermi volume does not change when going from the strongly intermediate valent regime all the way down to the QCP, where magnetic order sets in with a nearly trivalent Yb or Ce [7]. This has been confirmed experimentally by the observation of the ''large'' (f electron moves in valence band) Fermi-surface in a few Ce-based HF systems located just on the paramagnetic side of the QCP. In contrast, the ''small'' (f electron remains in

the f shell) Fermi surface has been observed in trivalent Ce compounds that lie well inside the magnetically ordered regime [8]. However, how the Fermi surface evolves upon crossing the QCP into the magnetically ordered ground state is not yet clear and hotly debated [9]. In the "SDW scenario" the $4f$ and the valence electron parts of the heavy quasiparticles at the Fermi surface (heavy electrons) remain tightly bound (composite fermions) and the onset of magnetic order just corresponds to the formation of a spin-density wave (SDW), similar to the case of $3d$ systems, e.g., Cr. The Fermi volume does not change, one merely expects a folding of the Brillouin zone (BZ) with a gap opening along the direction of the propagation vector. In contrast, in the so-called "local scenario" the composite fermions break up into the localized $4f$ and valence electron parts just at the QCP. Therefore, the volume of the Fermi surface is expected to shrink at the transition by one electron or one hole for Ce or Yb, respectively. Presently, there is theoretical and experimental support for either of these scenarios [9]. Likely the appropriate scenario might depend on the compound one is looking at. $YbRh_2Si_2$ is presently the compound which at ambient pressure, without doping, and without applied magnetic field, is closest to this QCP. Therefore this compound plays a central role in the debate "SDW" versus "local" scenario [9]. Its Fermi surface can be accessed by de Haas–van Alphen experiments [10], but only at high field which leads to a completely polarized state, where the large polarization of the $4f$ electrons affects strongly the FS and results in a seemingly "localized" (small) Fermi surface [11]. ARPES provides an alternative way to explore the Fermi surface at zero external field as a function of temperature. Thus ARPES studies of the Fermi surface of $YbRh_2Si_2$ are of strong relevance for the debate about the nature of the critical point in strongly correlated $4f$ systems, and for the more general question about the formation or break up of the composite fermions in Kondo lattice systems as a function of temperature or chemical doping.

Here we report on results of the FS mappings of the HF compound $YbRh_2Si_2$ by means of ARPES. As stated above, $YbRh_2Si_2$ [12] is very close to the QCP related to the disappearance of antiferromagnetic order upon increasing the hybridization between $4f$ and valence-band (VB) states. It is located just on the magnetic order side of this QCP, presenting a very well-defined, but very weak AF order below $T_N = 70$ mK. At $T > T_N$ pronounced deviations from Fermi-liquid behavior are observed up to temperatures of 10–15 K merging into a classical Kondo lattice behavior with a characteristic temperature, T_K, of 25 K. The present ARPES data were taken at ~10 K, a factor of 2 below T_K, and well below the onset of Kondo coherence which sets in below ~70 K. Thus one expects the composite fermions to be already partly formed. However, since $YbRh_2Si_2$ is located on the magnetic side of the QCP, and since the procedure how to calculate the Fermi surface in such a Kondo lattice at finite temperatures is rather unclear, we choose to discuss our ARPES data starting from LDA calculations for a purely trivalent Yb state and analyzing the effect of interaction between $4f$ and conduction electrons using a straightforward hybridization model.

ARPES experiments were performed at the Swiss Light Source (SIS instrument). Immediately before the measurements the sample was cleaved in ultrahigh vacuum conditions. Cleavage takes place between adjacent Si and Yb layers where the interlayer bonding is relatively weak. By inspection of the ARPES signal as a function of the beam position on the sample a surface region that was almost completely terminated by Si atoms was selected and then explored [13]. To discriminate between VB and $4f$ emissions, we used two photon energies: While at $h\nu = 45$ eV both kinds of states contribute to the measured signal, VB emissions are strongly suppressed at $h\nu = 110$ eV due to a Cooper minimum of the Rh $4d$ photoionization cross section [14].

ARPES data along the $\bar{\Gamma}$-$\bar{X}$ and $\bar{\Gamma}$-$\bar{M}$ directions of the surface BZ are shown in Fig. 1(a) and 1(b), respectively. The data show strongly dispersing bands mainly formed by

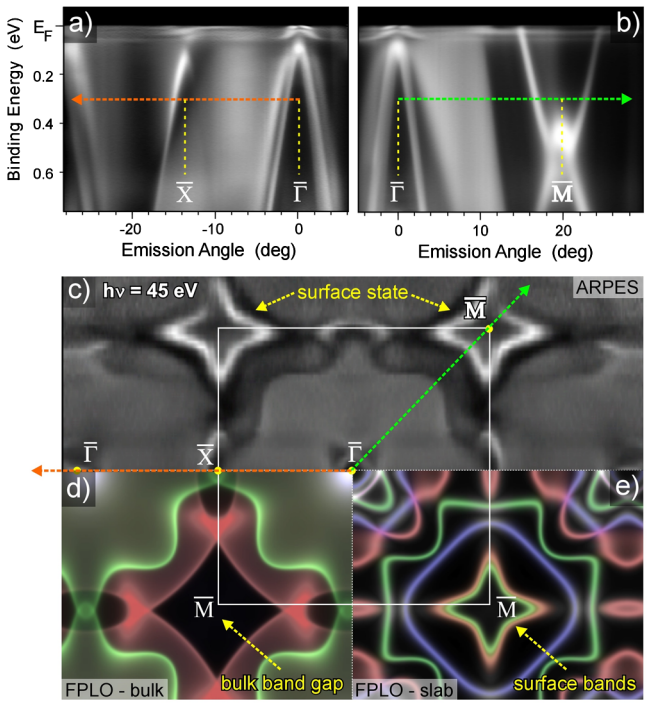

FIG. 1 (color online). (a) and (b) ARPES-derived band structure obtained with 45-eV photon energy taken along the $\bar{\Gamma}$-$\bar{X}$ and $\bar{\Gamma}$-$\bar{M}$ directions, respectively. (c) Isoenergy surface taken at 300 meV binding energy. Directions shown in (a), (b) are marked by arrows with broken lines. (d) Projected bulk bands from an FPLO band-structure calculation. Different colors denote different bands, brighter intensity indicates the presence of several states with different $\boldsymbol{k}_\perp$, but the same $\boldsymbol{k}_\parallel$. (e) Results of a slab calculation.

Rh 4d derived state, as well as a known bunch of crystal-field split Yb 4f states at E_F that reveal weak dispersions at points in $\boldsymbol{k}$ space where the VBs approach E_F and hybridize with the 4f states [15]. Before we come to the analysis of the Fermi surface, we will discuss the properties of an isoenergy surface at 0.3 eV binding energy, where f-d interactions are absent and experimental data are expected to be well described within LDA. Respective ARPES data are shown in Fig. 1(c) and reveal a fourfold symmetry as it is expected for the $YbRh_2Si_2(100)$ surface. A gray, almost homogeneously filled quadratic feature corresponding to emissions of intermediate intensity is centered around the $\bar{\Gamma}$ point. This area is surrounded by a region of lacking intensity and connected along the $\bar{\Gamma}$-$\bar{X}$ direction by narrow "necks" to respective features in the neighboring BZ. Around the $\bar{M}$ points sharp diamond-shaped features are observed, that are of high intensity, while close to the $\bar{M}$ point itself no photoemission (PE) intensity is recorded.

The experimental data are compared to results of LDA band-structure calculations using the FPLO [16] and LMTO [17] codes, that were projected along the $\boldsymbol{k}_z$ direction onto the (001) plane [Fig. 1(d)]. In both cases the theoretical results are very similar, in spite in the LMTO calculations Yb 4f states are treated as core states whereas in the FPLO calculations Yb atoms were substituted by Lu where 4f states lie at higher binding energy and do not influence the behavior of the valence bands close to E_F (in this case the calculated position of E_F was slightly shifted to achieve agreement with width and filling of the experimental VBs). The quadratic features around the $\bar{\Gamma}$ point as well as the connecting necks are properly reproduced by these calculations indicating that the respective structures stem from projected bulk bands responsible for a "donut"-shaped FS around the Z point of the bulk BZ [10]. Near the $\bar{M}$ points black regions indicate the presence of band gaps in the projected density of states (DOS). The experimentally observed bright diamonds are falling just within these gaps pointing to their nature as surface states. Figure 1(e) shows results of respective FPLO slab calculations that substantiate this conclusion. In fact, diamond-shaped surface states are found within the energy gaps around the $\bar{M}$ points.

Let us consider now an ARPES cut through the FS, i.e., an isoenergy surface at zero binding energy [Fig. 2(a)]. The diamond-shaped structures are still visible but now with increased size caused by an electronlike dispersion of the surface state that crosses E_F at the point $\bar{B}$ [cf. Fig. 2(e)]. Contrasting to Fig. 1(c) the quadratic features around the $\bar{\Gamma}$ point, except for this point itself, appear as black areas, i.e., regions of weak or even lacking PE intensity. These areas are surrounded by a sharp rather bright borderline that extends into the regions of the necks. The borderline obviously reflects emissions from the 4f-derived bands that reach E_F at the $\boldsymbol{k}$ point labeled $\bar{A}$ in Fig. 2(e). Between the $\bar{\Gamma}$ and the $\bar{A}$ point emission from VB states

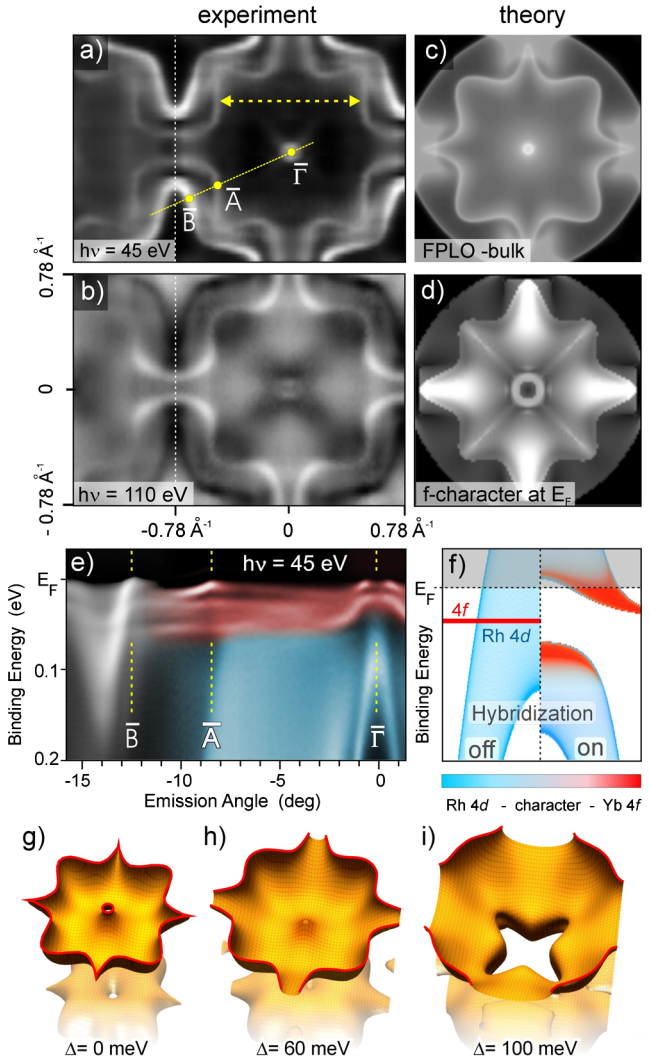

FIG. 2 (color online). (a) and (b) Fermi-surface cuts measured with 45-and 110-eV photon energies, respectively. Nesting regions are marked with arrows in (a). (c) Projected bands from bulk band-structure calculations. (d) 4f character contribution in the projected bulk bands as obtained from a calculation of $YbRh_2Si_2$ treating the 4f as a core states. To ease assignment of the FS sheets to particular electronic bands, the letters in (a) indicate certain points in the energy-momentum space that are depicted in (e). (f) Schematic presentation of changes in the electronic structure due to hybridization of extended VBs with a 4f state near the E_F. (g),(h), and (i) donut-shaped FS calculated within the hybridization model using parameter Δ equal to 0, 60, and 100 meV, respectively.

seems to vanish upon reaching the 4f states, leading to zero intensity at E_F in this region. Figure 2(c) shows results from the band-structure calculations described above, that do not differ considerably from those for the isoenergy surface shown in Fig. 1(d) and correlate with the small Fermi surface [10]. The calculations predict narrower necks and finite PE intensity within the quadratic regions around the $\bar{\Gamma}$ point, in disagreement with the ARPES data.

To explore the reason of the lacking intensity inside the sharp borderline and the nature of the latter, we repeated the FS mapping at $h\nu = 110$ eV [Fig. 2(b)], where ARPES data are dominated by emission from the Yb $4f$ states. Here, the discussed borderline is visible even better. Its intensity changes as a function of $\boldsymbol{k}$ reaching maximal values in the regions of the necks. The fact that the sharp borderline is visible both at 45 and 110 eV photon energies indicates its origin from f-d hybrid states.

Inside the borderline, finite ARPES signals ($h\nu = 110$ eV) are found that are particularly strong in the direction of the necks. This contribution stems not necessarily from the FS but might be derived from the weakly dispersive $4f$ bands observed close below E_F in Fig. 2(e). Respective contributions are not observed in Fig. 2(a) due to the better energy resolution at low photon energy ($h\nu = 45$ eV) that is smaller than the $4f$ binding energies. Finite $4f$ emissions are also found within the gaps of the projected band structure around the $\bar{M}$ point, surrounded by a sharp black borderline at those points in $\boldsymbol{k}$ space, where the surface state had been observed at $h\nu = 45$ eV. The appearance of $4f$ states within the gaps of the projected band structure is related to the localized, i.e., almost $\boldsymbol{k}$-independent character of these states, located closely below E_F. On the other hand, the disappearance of $4f$ emissions in the region of the surface state obviously reflects interaction with the latter.

The quenching of the VB emissions in Fig. 2(a) and the intensity variations of the $4f$ emission observed in Fig. 2(b) are obviously caused by f-d interactions. It was shown that this effect may be described within a simple hybridization model [15,18,19]. In this approach one starts from a dispersionless $4f^{13}$ state at binding energy ϵ that interacts with VBs via hopping interactions. The hybridization matrix element is assumed to be proportional to the f character of the valence states at the Yb site as obtained from a band-structure calculation, and the adjustable parameter Δ that describes the spatial overlap with the localized Yb $4f$ orbital. Applying this model to $YbRh_2Si_2$ allowed for a quantitative description of the observed $4f$ dispersion at the $\bar{\Gamma}$ point [15].

Figure 2(f) schematically shows hybridization effects on the energy distribution of the electron states projected along one direction in the BZ. Coupling leads to formation of a hybridization gap characterized by strong $4f$ admixtures to the lower and upper band edges and an upward dispersion of mainly $4f$ derived states just outside the region of the unhybridized VB. Depending on the chosen parameters, E_F lies either in the gap or intersects the upper band, so that FS should be very sensitive to the hybridization strength.

Application of this model to the realistic band-structure of $YbRh_2Si_2$ yields the following: Neglecting f-d hybridization ($\Delta = 0$) leads to the small FS with extremely narrow necks and a hole in the middle of the donut [Fig. 2(g)] which was also obtained by previous LDA calculations [10,20]. Analysis of the momentum character reveals considerable f contribution to the valence states that is particularly strong in the region of the necks [Fig. 2(d)] and fulfills, thus, the precondition for hybridization with $4f$ states. Neglecting the anisotropy of hybridization and choosing as model parameters $\epsilon = 10$ meV and $\Delta = 60$ meV leads to a FS with slightly larger diameter, broader necks but without the hole around the $\bar{\Gamma}$ point [Fig. 2(h)]. Further increase of Δ to a value 100 meV produces a broad crosslike hole around $\bar{\Gamma}$, combined with a huge opening of the necks [Fig. 2(i)]. While the hole predicted in this last scenario is in good agreement with the lacking intensity in Fig. 2(a) and, particularly, Fig. 2(b), the width of the necks is in conflict with our ARPES data. On the other hand, the shape of the necks is correctly described by the scenario shown in Fig. 2(h) that reproduces also previous results obtained within a renormalized band approach [21]. Additionally, $\Delta = 60$ meV for the bulk is consistent with $\Delta = 40$ meV at the surface reported in [15], where hybridization strength is estimated to be 70% of that of the bulk [22]. The observation of a holelike feature around the $\bar{\Gamma}$ point may be explained in this scenario by the fact that the hybridization gap providing this feature for $\Delta = 100$ meV decreases with decreasing Δ. For $\Delta = 60$ meV it does not affect the FS anymore, but influences the isoenergy surface a few meV below E_F. Since the energy resolution of the ARPES experiment averages over a window of about 10 meV, the small number of electron states between the FS and these isoenergy surfaces will lead to small intensities and thus an imaging of the hole-structure of the latter. The parallel alignment of the walls of the donut with the direction of projection, on the other hand, results in a strong increase of intensity reflected by the bright borderline.

Note that the topology of the FS exhibits significant nesting properties. Large portions of the borderline of the Fermi surface are running parallel to each other in the $\bar{\Gamma}$-$\bar{X}$ directions, as indicated by the double-side arrow in Fig. 2(a). One would expect favorable conditions for magnetic order (either of local or SDW type) with a propagation vector $\boldsymbol{Q}$ corresponding to the periodicity of the arrow, i.e., $\boldsymbol{Q} \sim (2/3, 0, 0)$. Unfortunately, the propagation vector of the AF state in $YbRh_2Si_2$ is still unknown and a comparison between theory and experiment is currently not possible. Whether the topology of the FS is conserved upon AF ordering at the QCP itself still remains an open issue and will certainly be a subject of further studies.

In summary.—Our study grants important insight into the structure of the Fermi surface of $YbRh_2Si_2$, the heavy-fermion compound that is closest to the QCP. The f-d hybridization of bulk states was found to cause a slight enlargement of the FS that extends up to the border of the BZ. But, except of closing a hole in the middle of donut the topology of the Fermi surface does not deviate much from

the donut-shaped, small FS, indicating that at 10 K f-d hybridization does not increase the Fermi volume significantly. On the other hand, our results reveal dramatic variations of the isoenergy surfaces near the FS on a scale of few meV due to the presence of a hybridization gap closely below E_F.

This work was supported by the DFG (grant VY64/1-1, GE602/2-1).

*vyalikh@physik.phy.tu-dresden.de

[1] N. E. Christensen *et al.*, J. Magn. Magn. Mater. **76–77**, 23 (1988); R. Ahuja *et al.*, Phys. Rev. B **50**, 11 183 (1994).
[2] C. N. Berglund and W. E. Spicer, Phys. Rev. **136**, A1030 (1964).
[3] Y. J. Chang *et al.*, Phys. Rev. B **81**, 235109 (2010).
[4] G. R. Stewart, Rev. Mod. Phys. **73**, 797 (2001); **78**, 743 (2006).
[5] P. W. Anderson, Phys. Rev. **124**, 41 (1961); O. Gunnarsson and K. Schönhammer, Phys. Rev. Lett. **50**, 604 (1983); Phys. Rev. B **28**, 4315 (1983).
[6] A. N. Tahvildar-Zadeh, M. Jarrell, and J. K. Freericks, Phys. Rev. Lett. **80**, 5168 (1998); M.-W. Xiao, Z. Z. Li, and W. Xu, Phys. Rev. B **65**, 235122 (2002).
[7] M. Oshikawa, Phys. Rev. Lett. **84**, 3370 (2000).
[8] M. Sugi *et al.*, Phys. Rev. Lett. **101**, 056401 (2008).
[9] P. Gegenwart, Q. Si, and F. Steglcih, Nature Phys. **4**, 186 (2008).
[10] P. M. C. Rourke *et al.*, Phys. Rev. Lett. **101**, 237205 (2008).
[11] K. Miyake and H. Ikeda, J. Phys. Soc. Jpn. **75**, 033704 (2006).
[12] J. Custers *et al.*, Nature (London) **424**, 524 (2003); O. Trovarelli *et al.*, Phys. Rev. Lett. **85**, 626 (2000); P. Gegenwart *et al.*, Phys. Rev. Lett. **89**, 056402 (2002).
[13] D. V. Vyalikh *et al.*, J. Electron Spectrosc. Relat. Phenom. **181**, 70 (2010).
[14] J. J. Yeh and I. Lindau, At. Data Nucl. Data Tables **32**, 1 (1985).
[15] D. V. Vyalikh *et al.*, Phys. Rev. Lett. **105**, 237601 (2010).
[16] K. Koepernik and H. Eschrig, Phys. Rev. B **59**, 1743 (1999).
[17] O. K. Andersen, Phys. Rev. B **12**, 3060 (1975).
[18] D. V. Vyalikh *et al.*, Phys. Rev. Lett. **100**, 056402 (2008).
[19] D. V. Vyalikh *et al.*, Phys. Rev. Lett. **103**, 137601 (2009).
[20] G. A. Wigger *et al.*, Phys. Rev. B **76**, 035106 (2007).
[21] G. Zwicknagl, J. Phys. Condens. Matter **23**, 094215 (2011).
[22] Yu. Kucherenko *et al.*, Phys. Rev. B **66**, 165438 (2002).